# Further Use of the Pressuremeter for Ground Improvement

## Nouvelles contributions du pressiomètre pour l'amélioration des sols

*Babak Hamidi*[1&2#]

[1]*Menard, Ground Improvement Lead, Perth, Australia*
[2]*ISSMGE TC-211, Chair*
[#]*Corresponding author: bhamidi@menard.com.au*

## ABSTRACT

Since its invention by the late French engineer, Louis Menard, the pressuremeter test (PMT) has been extensively used by geotechnical engineers and ground improvement specialists. This device has proven to be a reliable tool for measuring bearing capacity and settlements using formulas and methods that are dependent on PMT limit pressure and Menard modulus. However, the experience of the author indicates that it may have more use and can assist the geotechnical engineer and the ground improvement specialist in more ways. In this paper, the author describes how the pressuremeter can be used for assessing sand settlement under self-weight and proposes a method for performing a first approximation of post-dynamic compaction PMT parameters using data from a case study for verification.

## RESUME

Depuis son invention par le regretté ingénieur français Louis Menard, l'essai pressiométrique (PMT) a été largement utilisé par les ingénieurs géotechniciens et les spécialistes de l'amélioration des sols. Cet appareil s'est avéré être un outil fiable pour mesurer la capacité portante et les tassements, en utilisant des formules et méthodes dépendant de la pression limite du PMT et du module de Menard. Cependant, l'expérience de l'auteur suggère que cet outil pourrait avoir des applications supplémentaires et apporter une aide précieuse aux ingénieurs géotechniciens et spécialistes de l'amélioration des sols. Dans cet article, l'auteur décrit comment le pressiomètre peut être utilisé pour évaluer le tassement des sables sous leur propre poids et propose une méthode permettant d'effectuer une première approximation des paramètres PMT après compactage dynamique, à l'aide de données issues d'une étude de cas pour vérification.

**Keywords:** pressuremeter; PMT; ground improvement; self-bearing; self-weight; creep; dynamic compaction

## 1. Introduction

Louis Menard initially developed the prototype of the pressuremeter during his undergraduate studies at École des *Ponts et Chaussées* and later refined the device while completing his master's degree at the University of Illinois (Communication Department of Menard 2007).

After his academic achievements, Menard transitioned to his professional career by promoting the Menard pressuremeter test, frequently also called PMT. Menard's device was capable of directly assessing soil stress-strain behavior at various depths within a borehole, and soon gained recognition and widespread application in his home country of France and beyond, becoming instrumental for determining foundation bearing capacity and settlement using the pressuremeter limit pressure, $P_{LM}$, and Menard modulus, $E_M$ (Centre d'Études Menard 1975).

By 1969, Menard further advanced geotechnical practices by introducing dynamic compaction as a ground improvement technique, followed by the development of dynamic replacement (Hamidi 2014). Consequently, the PMT emerged as a vital tool for quality control testing in ground improvement projects, particularly for compact soils or crushed rock piers such as dynamic replacement columns and stone columns, where more commonly utilized tests like SPT (Standard Penetration Test) or CPT (Cone Penetration Test) are insufficient for penetration and evaluation.

While the pressuremeter is most commonly used to determine foundation bearing capacity and settlement, it has several additional applications. Among its uses are predicting soil creep without external loading and assessing improvements in mechanical properties as the soil densifies. These functions are highly beneficial for geotechnical engineers and ground improvement specialists.

## 2. Creep and aging due to self-weight of fill

Soil aging refers to the time-dependent changes in the properties of freshly deposited or disturbed soil when subjected to creep under a constant stress state (Liu et al. 2024).

Schmertmann (1991) provides examples of soil aging behavior, drawing from both laboratory and field studies across various soil types, including clays, silts, sands, and even gravel, over short and long periods.

Creep is the continuous deformation under constant stress over time. Becker et al. (2013) describe creep as a viscoelastic response to a constant deviator stress. Augusten et al. (2004) note that creep can be divided into three parts, namely

- Primary creep or transient creep, which is when strain rate decreases over time.
- Secondary creep or stationary creep, which is when strain rate is constant over time.
- Tertiary creep or acceleration creep, which is when strain rate increases over time.

Fig. 1 shows primary, secondary and tertiary creep over time in (a) cartesian plot and (b) log-log plot (Augusten et al. 2004).

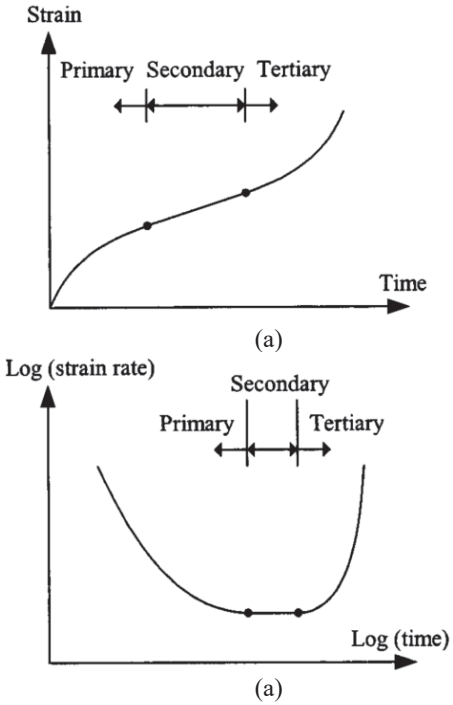


**Figure 1.** Creep in (a) cartesian plot and (b) log-log plot

During creep, sand particles undergo microstructural changes, such as interlocking and rearrangement, which contribute to aging (Liu et al. 2024). Factors like wetting, vibrations, or temporary reductions in shear resistance at grain contact points can accelerate this process and lead to further soil compaction (Centre d'Études Menard 1975).

These microstructural changes increase small-strain stiffness, strength, and cone penetration resistance, thereby increasing soil stability (Schmertmann 1991, Liu et al., 2024). However, creep resulting from the self-weight of young and compressible fills can cause significant long-term settlements, potentially compromising structures built on such soils without adequate ground improvement or sufficient time for the soil to age and strengthen.

Augusten et al. (2004) explain by analogy that time-dependent behavior of granular soils at low confining stresses are caused by rearrangement over time due to sliding and rolling between the sand particles and behavior at high confining stresses deformations are associated with continuous fracturing, crushing and deformation of the grains.

Augusten et al. (2004) point out that experimental results show that creep strains are not negligible and can reach 10% of the monotonic loading strain.

The concept of soil self-bearing capacity, or soil ability to resist settling under its own weight, is governed by specific physical and mechanical properties, and Menard recognized limit pressure as a reliable indicator of this capacity (Centre d'Études Menard 1975).

Table 1 outlines the required net limit pressure, $P_{LM}{}^{*}$, for soils at depths of less than 10 m to achieve self-bearing conditions.

$P_{LM}{}^{*}$ is defined in Eq. (1).

$$P_{LM}{}^{*} = P_{LM} - P_o \tag{1}$$

Where $P_o$ is the at rest horizonal pressure of the soil.

This table accounts for external variables, including fluctuations in the water table, seasonal changes in moisture, and vibrations from road traffic. The values shown in Table 1 must be increased for soil at depths exceeding 10 m.

**Table 1.** Required $P^{*}_{LM}$ for self-bearing condition (Centre d'Etudes Menard, 1975)

| Soil type | $P_{LM}$ (kPa) for self-bearing condition | $\alpha$ |
|---|---|---|
| **Clay** | 250 to 300 | 2/3 |
| **Silt** | 400 | 1/2 |
| **Sand** | 600 | 1/3 |
| **Sand & gravel** | 800 | 1/4 |

The author notes that there is a discrepancy in the parameter that should be used in Table 1. Although Menard states that the Table is based on *net* limit pressure, in his discussion for a first approximation of one-year settlement of any soft layer he proposes a function of limit pressure (in kPa units) as shown in Eq. (2).

$$s = \frac{h}{1000} \times \frac{1 - \alpha \frac{P_{LM}}{200}}{\alpha \frac{P_{LM}}{200}} \tag{2}$$

With a condition that

$$P_{LM} < \frac{200}{\alpha} \text{ (kPa)} \tag{3}$$

$s$=one year settlement (cm)

$\alpha$ = rheological factor shown in Table 1 (Centre d'Études Menard 1975).

$h$= thickness of layer (in cm)

Replacement of $\alpha$ values in Eq. (3) yields values shown in Table 1 and Eq. (2) will result in no creep when $P_{LM}$ equals to the value shown in Table 1; hence, the parameter in Table 1 and Eq. (2) and Eq. (3) must be the same, i.e., they must either be $P_{LM}{}^{*}$ or $P_{LM}$.

## 3. Influence of soil straining of strength

Menard (Centre d'Études Menard 1975) notes that straining the soil and increasing its density will increase the soil's limit pressure and proposes Eq. (4).

$$P_{LM1} = \beta P_{LM0} \quad (4)$$

$P_{LM1}$ = limit pressure immediately after densification

$P_{LM0}$ = limit pressure immediately before densification

$\beta$= coefficient that depends on the soil type and amount of compaction

**Table 2.** $\beta$ values (Centre d'Etudes Menard, 1975)

| Percentage of compaction | Sand | Silt | Clay |
|---|---|---|---|
| **1%** | 1.3 | 1.2 | 1.1 |
| **2%** | 1.5 | 1.4 | 1.2 |
| **4%** | 2.0 | 1.6 | 1.3 |

Based on personal discussions between Menard and Varaksin, Varaksin et al (2005) proposed that 3% strain in young dune sand fills will double $P_{LM}$.

On the above basis, Hamidi et al. (2010a) suggest that in sands

$\varepsilon$= strain

$(P_{LM})_i$= limit pressure before soil improvement

$(P_{LM})_j$= limit pressure after soil improvement

$n$= number of times limit pressure doubles

$a$= percentage of strain induced for doubling i.e., 4% from Table 2 or 3% from Varaksin et al. (2005), then:

$$\varepsilon = na \quad (5)$$

$$(P_{LM})_j/(P_{LM})_i = 2^n \quad (6)$$

Then solving Eq. (6) for $n$, and replacing its result in Eq. (5) will yield:

$$\varepsilon = \frac{\log\left((P_{LM})_j/(P_{LM})_i\right)}{\log 2} a \quad (7)$$

Settlement, $S$, that is induced by straining or densification can be calculated to be:

$$S = \sum_{k=1,m} S_k = \sum_{k=1,m} h_k \varepsilon_k \quad (8)$$

$$S = \frac{a}{\log\ 2} \sum_{k=1,m} h_k \log\left( {(P_{LM})_j}/{(P_{LM})_i} \right)_k \quad (9)$$

$m$= number of layers that have been tested

$h_k$= layer thickness

Eq. (9) can be used as a first approximation to estimate creep settlement of sand or the settlement induced by ground improvement efforts.

In the first scenario, it is sufficient to compare the soil's existing limit pressure with the self-bearing threshold of 600 kPa, as presented in Table 2. Layers with in-situ limit pressure values exceeding 600 kPa will not contribute to creep. However, layers with lower limit pressure values will contribute to creep settlement, which can be calculated using Eq. (9).

Similarly, ground improvement induced settlement can be estimated by utilizing post and pre ground improvement limit pressure ratios in Eq. (9).

## 4. Predicting PMT parameters using dynamic compaction induced subsidence

Dynamic compaction (DC), pioneered and promoted by Louis Menard, is a widely used ground improvement method since the early 1970s (Hamidi et al. 2009). It involves the repeated dropping of a heavy weight, referred to as a pounder or tamper, from a significant height to densify soil at substantial depths. The process typically comprises multiple drops on the same point, followed by sequential drops on other points arranged in a predetermined grid. This treatment is executed in at least two deep compaction phases, followed by a lighter energy phase known as ironing.

The soil improvement achieved through dynamic compaction results in ground subsidence. The magnitude of induced settlement is not considered an acceptance criterion because it is only indicative of the amount of improvement but does not directly quantify it. Contemporary best practice stipulates verification of ground conditions through PMT or other suitable tests to confirm compliance with project specifications.

Research by Hamidi et al. (2010b, 2011) suggests that DC induced settlement may provide a preliminary estimate of improved pressuremeter parameters, offering additional insight into the outcomes of the technique.

Several studies indicate that soil displacement induced by dynamic compaction often exhibits a sickle-shaped pattern. Lukas (1986, 1995) conducted measurements of lateral soil movement across three different soil types. As shown in Fig. 2, his observations reveal that ground movement initially increases from the surface to a certain depth, beyond which it diminishes until further changes become negligible.

Bonab and Rezaei (2009) demonstrated similar findings in their laboratory-scale DC experiments, employing particle image velocimetry (PIV) techniques. Their results, which are shown in Fig. 3 revealed that soil displacement profiles along vertical lines exhibit a sickle-shaped curve, which flattens progressively with increasing distance from the impact center. Additionally, the displacement of soil within horizontal planes was observed to form a bell-shaped curve.

A relationship between strain (or induced settlement) and changes in limit pressure has already been established, so if DC induced settlement and initial limit pressure values are known it may be possible to estimate post compaction limit pressure if the strain profile can be estimated.

Eq. (6) to Eq. (9) demonstrate the relationship between strain, manifested as induced settlement, and changes in limit pressure. Consequently, if the induced settlement and initial limit pressure values resulting from dynamic compaction (DC) are known, it becomes feasible to estimate post-compaction limit pressure, provided the strain profile can be determined.

The (net) equivalent limit pressure, utilized in bearing capacity calculations, is derived as the geometric mean of values measured across three zones: from $+3R$ to $+R$

above the founding level, +*R* to -*R*, and -*R* to -3*R*, where *R* represents the footing equivalent radius (Centre d'Études Menard 1975). Although point-by-point post-treatment $P_{LM}$ estimation results may deviate from actual conditions, the impact on bearing capacity calculations is expected to remain within acceptable margins for a first approximation, provided the overall profile aligns with reality.

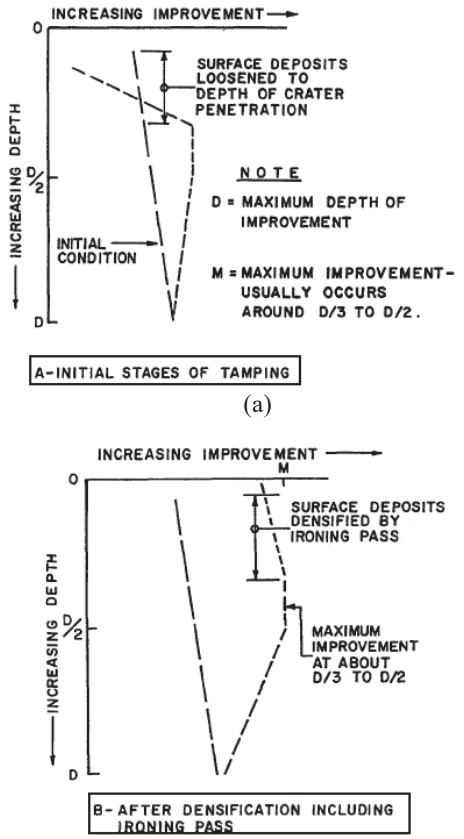


**Figure 2.** Variation in improvement with depth during Dynamic Compaction (a) Deep treatment without ironing (b) treatment with ironing

Berry et al. (2004) proposed a continuous Rayleigh distribution, presented in the form of Eq. (10) and shown in Fig. 4a, to model void ratio reduction during impact roller compaction. This technique applies impact energy at the surface and demonstrates results comparable to DC, albeit at a smaller scale.

$$f(z) = \frac{z}{\sigma^2} e^{-z^2/2\sigma^2} \quad (10)$$

z= depth from surface

σ= depth of maximum strain.

Lukas (1986, 1995) assumes maximum improvement to be at a depth between 1/3 to 1/2 of the depth of improvement.

The drawback of the Rayleigh distribution is the curve starts at zero strain, which does not conform with reality, and the model will predict low PMT parameters in the upper layers.

The author suggests a shifted Rayleigh distribution, as presented in Eq. (11) and shown in Fig. 4b and Fig 4c.

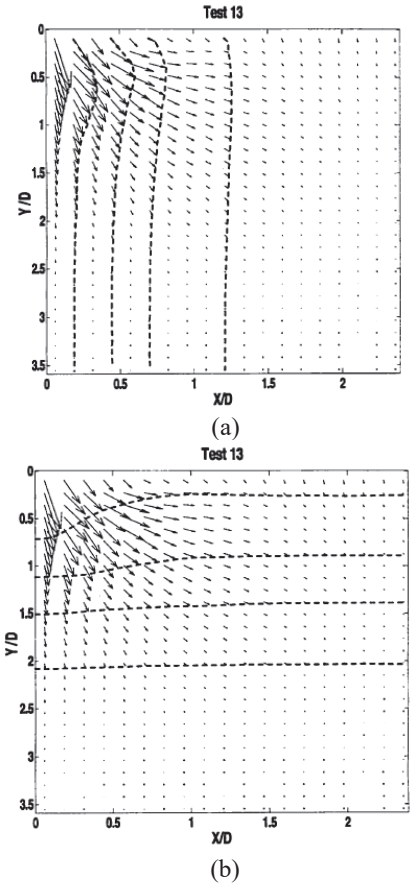


**Figure 3.** Normalized displacement vectors after 10th impact for (a) vertical lines and (b) horizontal lines of soil (D= pounder diameter) (Bonab and Rezaei 2009)

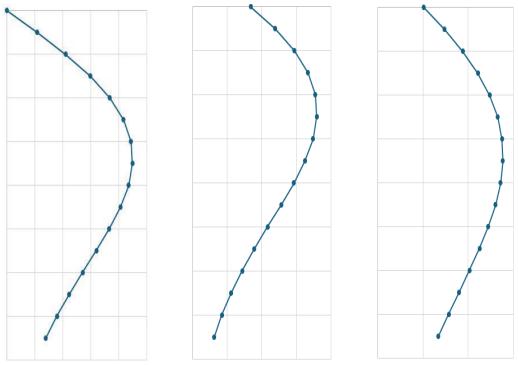


**Figure 4.** Strain profile using (a) Rayleigh distribution, (b) shifted Rayleigh distribution (c) shifted Rayleigh distribution with maximum strain depth also shifted downwards

$$f(z) = \frac{z - C}{\sigma^2} e^{-(z-C)^2/2\sigma^2} \quad (11)$$

Where *C*= initial or shift value

Hamidi et al. (2010b, 2011) also used Eq. (10) to develop a strain model for dynamic compaction. In that model it was assumed that not only did strain and settlement distribution follow the curve of Eq. (10), but also the amount of strain and settlement in the layers were as per Eq. (10).

While during verification process it appeared that $P_{LM}$ geometric mean was within reason, the author now understands that Eq. (10) is the PDF (Probability Density Function). The settlement and strain of the layers follow Rayleigh's distribution, and the curve represents how settlement is distributed across depth. However, Rayleigh distribution is continuous, meaning it has infinitely possible values between any two depths.

The PDF curve does not present the strain or settlement at any single depth; the settlement or strain of the layer can be calculated as the area under the curve with the increment's thickness multiplied by its instantaneous strain. When the increments are very small, this will be the integral of PDF, which is the CDF (Cumulative Distribution Function). For the distribution function presented in Eq. (11) CDF will be as shown in Eq. (12).

$$F(z) = 1 - e^{-(z-C)^2/2\sigma^2} \tag{12}$$

The difference between $F(z)$ of two depths $z_2$ and $z_1$ is the area under the PDF and is its value is the percentage of area compared to the total area under PDF that is 1.

The percentage of settlement or strain, $P$, in a depth interval compared to total settlement or strain will be

$$P = F(z_2) - F(z_1) \tag{13}$$

In the proposed model it is assumed that:

- Initial $P_{LM}$ values are known.
- Total DC induced ground settlement is known.
- Settlement follows shifted Rayleigh's distribution.
- $P_{LM}$ values are reasonably in the same range, i.e., there are not any very dense layers that would not be predictable by a Rayleigh distribution.

If $\varepsilon_{DC\_k}$= DC induced strain in layer $k$ (testing interval), then Eq. (8) can be rewritten as:

$$S = \sum_{k=1,m} S_k = \sum_{k=1,m} h_k \varepsilon_{DC\_k} \tag{14}$$

Where $h_k$= testing interval

If pre-treatment $P_{LM}$ values were uniform across all testing depths, it could be inferred that DC imposes strain on each soil layer in such a way that final ground strain will be reasonably similar to shifted Rayleigh distribution.

In most practical cases, $P_{LM}$ values are expected to vary between intervals. To account for this variability, it can be imagined that all soil layers initially had the same $P_{LM}$ value but were pre-strained by $\varepsilon_{o\_k}$ and underwent a pre-settlement $S_0$ to reach their pre-DC state.

Upon DC treatment, the soil will experience additional strain, $\varepsilon_{DC\_k}$, and the strain profile is assumed to conform to the shifted Rayleigh distribution. The combined effect of $\varepsilon_{o\_k}$ and $\varepsilon_{DC\_k}$ constitutes the shifted Rayleigh distribution strain, $\varepsilon_{R\_k}$ and is shown in Fig. 5.

$$\varepsilon_{o\_k} + \varepsilon_{DC\_k} = \varepsilon_{R\_k} \tag{15}$$

Equivalently, for settlements:

$$S_{o\_k} + S_{DC\_k} = S_{R\_k} \tag{16}$$

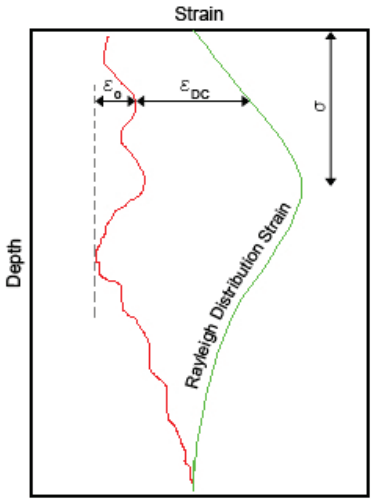


**Figure 5.** Shifted Rayleigh distribution of strain as a function of pre-treatment and DC induced strain (Hamidi et al 2010b)

$S_{o\_k}$= settlement relating to $\varepsilon_{o\_k}$

$S_{DC\_k}$= settlement relating to $\varepsilon_{DC\_k}$.

By adding all layers in Eq. (16):

$$\sum S_{0\_k} + \sum S_{DC\_k} = \sum S_{R\_k} = S_R \tag{17}$$

$$\sum S_{0\_k} + S_{DC} = S_R \tag{18}$$

$S_{o\_k}$ is known for each layer:

$$S_{o\_k} = \frac{\log\left(P_{LM\_k}/P_{LM\_min}\right)}{\log 2} a h_k \tag{19}$$

$S_{DC\_k}$ is not known. However, total settlement DC induced, $S_{DC}$, is known from site measurements and $S_R$ can be calculated from Eq. (18). Therefore, it is possible to calculate $S_{DC\_K}$ for each layer as:

$$S_{DC\_k} = PS_{Rk} - S_{o\_k} \tag{20}$$

It is noted that Rayleigh distribution extends further than testing depth; hence the settlement percentages calculated using Eq. (13) for the layers will not be 100%. Therefore, $S_o$ and $S_{DC}$ should be adjusted to the percentages within the depths of discussion.

$\varepsilon_{DC\_k}$ can be calculated from Eq. (21):

$$\varepsilon_{DC\_k} = S_{DC_k}/h_k \tag{21}$$

As a final step, using Eq. (5) and Eq. (6) in conjunction with Eq. (21), post improvement $P_{LM}$ of each layer can be computed to be:

$$\left(P_{LM\_k}\right)_{post} = \left(P_{LM\_k}\right)_{pre} 2^{\varepsilon_{DC\_k}/a} \tag{22}$$

As can be seen in Fig. 4b, in shifted Rayleigh distribution, maximum depth of strain will shift upwards (for negative values of $C$). Therefore, $\sigma$ can be assumed to range arbitrarily between one-third and one-half of the depth of influence after applying $C$, i.e., its value will be shifted downwards to balance the upward shift by $C$. This is shown in Fig. 4c.

Menard (Centre d'Études Menard 1975) established a linear correlation between $P_{LM}$ and $E_M$ for various soil types. Building on this relationship, it is reasonable to hypothesize that a similar approach could be employed to estimate post-DC $E_M$ values. It can be assumed that, for sands, The $E_M$ doubles each time the soil is subjected to a strain of a certain percentage, $b$, which does not necessarily need to be $a$ (although, at this stage, it would be rational to assume they are equal since the relationship between $P_{LM}$ and $E_M$ is linear). Consequently, the same process can be followed if $P_{LM}$ is replaced by $E_M$ in the previous equations.

## 5. Verification of model

Al Quoa'a, a remote desert township in the United Arab Emirates, presented unique geotechnical challenges. In the first phase of construction, desert dune sands were leveled without compaction to create a flat construction platform, which led to deep cracking in buildings built on fill areas.

In response to these issues, the second phase of the project involved constructing a non-engineered fill platform spanning approximately 1.13 million m², with a maximum fill thickness of 28 m. A design-and-build methodology was employed (Hamidi et al. 2010a), incorporating tailored design and acceptance criteria to align with project requirements. Dynamic compaction was implemented to enhance bearing capacity and mitigate total, differential, and creep settlements within the contractual timeframe of 10 months.

The development of design criteria (Table 3) was guided by the necessity to improve bearing capacity and restrict settlements to acceptable levels for building and infrastructure performance. Importantly, onerous criteria were not extended to excessive depths beyond the reach of imposed stresses. This ensured that the fill remained sufficiently stable without creeping to meet the project's requirements

**Table 3.** Acceptance criteria (Hamidi et al. 2010a)

| Design Criteria | Villa areas | Non-villa areas |
|---|---|---|
| **Bearing capacity** | 200 kPa at depth of 0.75 m | 100 kPa at depth of 0.75 m |
| **Total settlement** | 25 mm | 25 mm |
| **angular distortion** | 1/1250 | 1/1250 |
| **Creep settlement** | To be eliminated | To be eliminated |

Consequently, acceptance criteria were defined based on PMT as shown in Table 4 and Table 5 (Hamidi et al 2010a).

**Table 4.** Acceptance criteria for villa areas

| Criteria | Safe bearing | Self-bearing |
|---|---|---|
| **Depth (m)** | 0.75 to 5.5 | Deeper than 5.50 |
| **$P_{LM}$ (kPa)** | 750 | 600 |
| **$E_M$ (MPa)** | 4.8 | 4.0 |

**Table 5.** Acceptance criteria for non-villa areas

| Criteria | Safe bearing | Self-bearing |
|---|---|---|
| **Depth (m)** | From 0.0 | From 0.0 |
| **$P_{LM}$ (kPa)** | 600 | 600 |
| **$E_M$ (MPa)** | 4.0 | 4.0 |

Dynamic compaction was performed using 15-, 25- and 35-ton pounders. Fig. 6 shows the MARS (Menard Automatic Release System) 35-ton pounder being dropped in free fall and automatically reconnecting without manual intervention.

**Figure 6.** Application of DC using 35-t pounder (Hamidi et al. 2010a)

PMTs were conducted to assess the effectiveness of the ground improvement measures. The pre- and post-treatment limit pressures for a representative test location are shown in Fig. 7, while $P_{LM}$ values are also presented in Table 6. Additional test results and further analysis can be found in Hamidi et al. (2010a), offering a broader perspective on the success of the implemented technique.

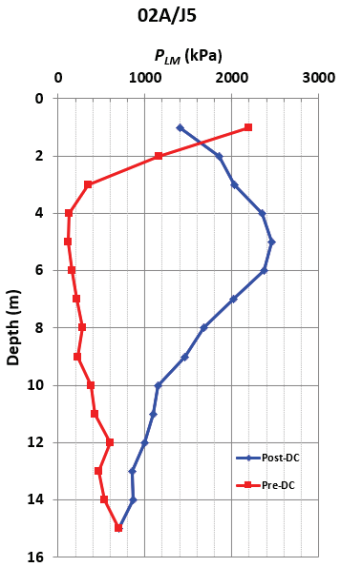


**Figure 7.** Pre- and post-dynamic compaction limit pressures (Hamidi et al. 2010a)

It can be observed that, aside from the top 2 m of compacted sand, the remaining soil was relatively loose, with $P_{LM}$ values typically ranging between 120 and 400 kPa. These low values suggest that the sand was prone to settlement under its own weight, a phenomenon previously responsible for building cracks during the project's initial phase.

The self-weight settlement of the sand can be estimated using Eq. (9), as detailed in Table 6. The calculations presented in this table are based on $P_{LM}$ values. For the sand layer to remain stable and avoid creeping under its self-weight, the $P_{LM}$ value must exceed 600 kPa. When values are above this threshold, the sand layer remains stable and does not contribute to settlement creep.

Table 6 estimates the self-weight settlement to range from 385 mm to 514 mm, using $a$ value of 3% and 4%. These findings suggest that the sand may exhibit strain ranging from 2.5% to 3.4% under its own weight.

The author has performed the same estimation process using $P_{LM}^*$ values, which is presented in Table 7. This calculation is more cumbersome as calculation of $P_{LM}^*$ requires the determination of $P_o$ for each layer, which in turn needs knowledge of the unit weight, $\gamma$, and internal friction angle, $\varphi'$, of each layer, see Eq. (27).

$$P_o = k_o \sigma_v = (1 - \sin\varphi')\gamma H \quad (27)$$

$k_o$ = coefficient of lateral earth pressure at rest, estimated using Jaky's (1948) method.

Neither $\gamma$ nor $\varphi'$, are known. Based on experience, as a first estimate the author has chosen unit weights of 18 and 16.5 kN/m$^3$ when limit pressures were respectively greater than or less than 600 kPa.

**Table 6.** Estimation of self-weight settlement using $P_{LM}$

| Depth (m) | $P_{LM}$ (kPa) | | | Estimated Creep (m) Eq. (8) based on $P_{LM}$ | |
|---|---|---|---|---|---|
| | Pre-DC | Post-DC | self-bearing | a= 3% | a=4% |
| **1** | 2200 | 1400 | 600 | 0.000 | 0.000 |
| **2** | 1160 | 1860 | 600 | 0.000 | 0.000 |
| **3** | 350 | 2030 | 600 | 0.023 | 0.031 |
| **4** | 130 | 2350 | 600 | 0.066 | 0.088 |
| **5** | 120 | 2460 | 600 | 0.070 | 0.093 |
| **6** | 160 | 2370 | 600 | 0.057 | 0.076 |
| **7** | 220 | 2020 | 600 | 0.043 | 0.058 |
| **8** | 280 | 1680 | 600 | 0.033 | 0.044 |
| **9** | 230 | 1460 | 600 | 0.041 | 0.055 |
| **10** | 380 | 1150 | 600 | 0.020 | 0.026 |
| **11** | 420 | 1100 | 600 | 0.015 | 0.021 |
| **12** | 600 | 1000 | 600 | 0.000 | 0.000 |
| **13** | 470 | 850 | 600 | 0.011 | 0.014 |
| **14** | 530 | 860 | 600 | 0.005 | 0.007 |
| **15** | 700 | 704 | 600 | 0.000 | 0.000 |
| | | | Creep= | 0.385 | 0.514 |

$\varphi'$ can be estimated using Eq. (28) (Etude Pressiometrique Louis Menard (1970) cited by Baguelin et al. (1978), which itself is dependent on $P_{LM}^*$.

$$P_{LM}{}^* = 2.5 \times 2^{\frac{\varphi' - 24}{4}} \quad (28)$$

An iterative process can be used for calculating $P_{LM}^*$ and $\varphi'$ using Eq. (27) and Eq. (28) with sufficient convergence in approximately three iterations.

Creep has been recalculated in Table 7 using $P_{LM}^*$ as the basis of formulation.

Table 7 estimates the self-weight settlement to range from 577 mm to 769 mm, using $a$ value of 3% and 4%. These results indicate that the sand may experience strain ranging from 3.8% to 5% under its own weight. It is evident that the estimated creep value has increased. This could have been anticipated, as the threshold value of 600 kPa in the numerator of the ratio remains constant, while the $P_{LM}^*$ value in the denominator is lower than $P_{LM}$.

**Table 7.** Estimation of self-weight settlement using $P_{LM}^*$

| Depth (m) | Pre-DC $P_{LM}$ (kPa) | $\varphi'$ (°) | $P_o$ (kPa) | $P_{LM}^*$ (kPa) | Estimated Creep (m) Eq. (8) based on $P_{LM}^*$ | |
|---|---|---|---|---|---|---|
| | | | | | 3% | 4% |
| **1** | 2200 | 36.5 | 7.3 | 2192.7 | 0.000 | 0.000 |
| **2** | 1160 | 32.8 | 16.5 | 1143.5 | 0.000 | 0.000 |
| **3** | 350 | 25.5 | 28.2 | 321.8 | 0.027 | 0.036 |
| **4** | 130 | 17.7 | 45.9 | 84.6 | 0.085 | 0.113 |
| **5** | 120 | 15.9 | 59.9 | 61.4 | 0.099 | 0.132 |
| **6** | 160 | 18.3 | 67.9 | 93.0 | 0.081 | 0.108 |
| **7** | 220 | 20.9 | 74.3 | 146.2 | 0.061 | 0.081 |
| **8** | 280 | 22.7 | 81.1 | 199.2 | 0.048 | 0.064 |
| **9** | 230 | 20.4 | 96.7 | 134.3 | 0.065 | 0.086 |
| **10** | 380 | 24.7 | 96.0 | 284.1 | 0.032 | 0.043 |
| **11** | 420 | 25.4 | 103.8 | 316.2 | 0.028 | 0.037 |
| **12** | 600 | 27.9 | 105.2 | 494.4 | 0.008 | 0.011 |
| **13** | 470 | 25.9 | 120.7 | 349.1 | 0.023 | 0.031 |
| **14** | 530 | 26.8 | 127.0 | 402.7 | 0.017 | 0.023 |
| **15** | 700 | 28.7 | 140.5 | 559.7 | 0.003 | 0.004 |
| | | | | Creep= | 0.577 | 0.769 |

To verify the applicability of the model it is assumed that DC induced compaction is the result of $P_{LM}$ doubling for $a$= 3%, which will yield 0.86 m. This assumption will eliminate any errors that may be introduced in the model due to the impact of $a$, i.e., because assumed induced and predicted DC strains and settlements are on the same basis, the results will not be dependent on the value of $a$.

**Table 8.** Estimation of self-weight settlement using $P_{LM}^*$

| D | PLM (kPa) Actual Values | | $S_0$ | $P$ | $PS_R$ | $S_{DC}$ | $P_{LM}$ (kPa) Est. |
|---|---|---|---|---|---|---|---|
| m | Pre-DC | Post-DC | (m) | (%) | (m) | (m) | Post-DC |
| **1** | 2200 | 1400 | 0.13 | 4.5 | 0.09 | -0.04 | 946 |
| **2** | 1160 | 1860 | 0.10 | 5.3 | 0.11 | 0.01 | 1378 |
| **3** | 350 | 2030 | 0.05 | 5.9 | 0.12 | 0.07 | 1853 |
| **5** | 120 | 2460 | 0.00 | 6.6 | 0.13 | 0.13 | 2287 |
| **6** | 160 | 2370 | 0.01 | 6.7 | 0.13 | 0.12 | 2588 |
| **7** | 220 | 2020 | 0.03 | 6.7 | 0.13 | 0.11 | 2693 |
| **8** | 280 | 1680 | 0.04 | 6.4 | 0.13 | 0.09 | 2597 |
| **9** | 230 | 1460 | 0.03 | 6.1 | 0.12 | 0.09 | 2342 |
| **10** | 380 | 1150 | 0.05 | 5.7 | 0.11 | 0.06 | 1999 |
| **11** | 420 | 1100 | 0.05 | 5.2 | 0.10 | 0.05 | 1635 |
| **12** | 600 | 1000 | 0.07 | 4.6 | 0.09 | 0.02 | 1298 |
| **13** | 470 | 850 | 0.06 | 4.1 | 0.08 | 0.02 | 1013 |
| **14** | 530 | 860 | 0.06 | 3.5 | 0.07 | 0.01 | 786 |
| **15** | 700 | 704 | 0.08 | 3.0 | 0.06 | -0.02 | 612 |

Calculations for estimating post DC $P_{LM}$ are shown in Table 8. In the calculations it was assumed that $C$= -3.5 $\sigma$= 9. These values were derived by plotting Rayleigh PDF and CDF with the intent of identifying a depth of maximum strain that would be within DC expectation.

$S_0$ was calculated using Eq. (19) with $P_{LM\_min}$= 120 kPa at depth of 5 m.

$P$ is calculated using Eq. (12) and Eq. (13).

$S_R$ is calculated using Eq. (19). It is noted that the value of $S_R$ that has been used in the Table is the summation of $S_0$ values from Table 8 (0.75 m) and $S_{DC}$ (0.86). The total was then divided by total summation of $P$ values (80.6%) in Table 8 with consideration that calculations are only for depths within the table.

Once $S_{DC}$ has been calculated from Eq. (20) for each layer, the associated $P_{LM\text{-}DC}$ can be estimated from Eq. (22). This is shown and compared to actual post-DC $P_{LM}$ in Fig. 8. Although differences can be observed between the two curves, the geometric mean values for actual and predicted post-DC were both 1438 kPa.

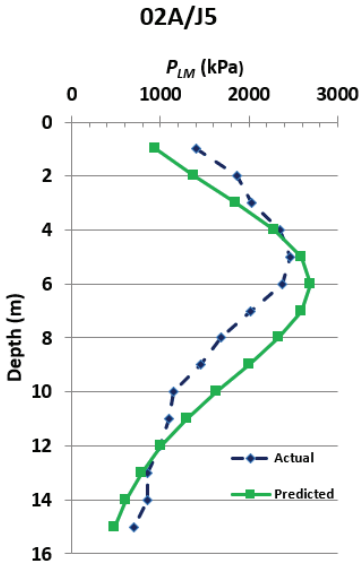


**Figure 8.** Pre- Actual and predicted post-DC $P_{LM}$ values.

The author has trialled various values for $C$ and $\sigma$. These resulted in post-DC $P_{LM}$ curves that sometimes were very different from the actual profile, but the geometric mean remained the same.

## 6. Conclusions

This study explores the extended application of the pressuremeter in ground improvement. A method is proposed for approximating creep or settlement of sand under self-weight, utilizing threshold values of limit pressure and the relationship between strain and the ratio of limit pressure increase. Additionally, a preliminary approach is introduced to estimate the geometric mean of limit pressure following dynamic compaction, based on pre-compaction limit pressure values and dynamically induced ground settlement. The findings suggest that the proposed methodology yields reasonable results within the scope of this research. Further investigation is recommended to refine the correlation between strain and limit pressure enhancement, as it plays a pivotal role in advancing the proposed framework.

## References


Augustesen, A, M A Liingaard, and P V Lade. 2004. "Evaluation of Time-Dependent Behavior of Soils." *International Journal of Geomechanics, ASCE* 4 (3): 137–156.

Becker, T. S., Dove, J. E. and Dove, P. M. 2013. "Experimental Creep Behaviour and Modelling of Silicified Sand." Ground Improvement, ICE Proceedings 166 (GI2): 115-124.

Baguelin, F., Jezequel, J. F. and Shields, D. H. 1978. "The Pressuremeter and Foundation Engineering". Aedermannsdorf, Trans Tech Publications, 617.

Berry, A., Visser, A. and Rust, E. 2004. "A Simple Method to Predict the Profile of Improvement after Compaction using Surface Settlement". In *Int Symp on Ground Improvement*, Paris, 9-10 September 2004, pp. 371-386.

Bonab, M. H. and Rezaei, A. H. 2009. "Physical Modelling of Low-Energy Dynamic Compaction", Int J of Physical Modelling in Geotechnics, Vol. 3, pp. 21-32.

Centre d'Etudes Menard. 1975. "The Menard Pressuremeter, D60." *Sols Soils* (26): 5-43.

Communication Department of Menard. 2007. *Menard - Half a Century of History - Un Demi Siècle D'histoire.* Mame à Tours.

Etude Pressiometrique Louis Menard. 1970. "Détermination De La Pousée Exercée Par Un Sol Sur Une Pario De Soutènement, D38/70."

Hamidi, B. 2014. "Distinguished Ground Improvement Projects by Dynamic Compaction or Dynamic Replacement", PhD, Curtin University.

Hamidi, B., Nikraz, H. and Varaksin, S. 2009. "A Review on Impact Oriented Ground Improvement Techniques." Australian Geomechanics 44 (2): 17-24.

Hamidi, B, H Nikraz, and S Varaksin. 2010a. "Soil Improvement of a Very Thick and Large Fill by Dynamic Compaction." In *3rd Int Conf on Problematic Soils (PS10), Adelaide, 7-9 April*.

Hamidi, B., Varaksin, S. and Nikraz, H. 2010b. "Predicting Soil Parameters by Modelling Dynamic Compaction Induced Subsidence." In *6th Australasian Congress on Applied Mechanics (ACAM6)*, Perth, Australia, 12-15 December, Paper 1150.

Hamidi, B., Varaksin, S. and Nikraz, H. 2011. "Predicting Menard Modulus using Dynamic Compaction Induced Subsidence." In *Int Conf on Advances in Geotechnical Engineering (ICAGE)*, Perth, 7-11 November: 221-226.

Jaky, J. 1948. "Pressure in silos." In *2nd Int Conf on Soil Mechanics and Foundation Engineering.* 1: 103-107.

Liu, B, J Xue, B M Lehane, and Z Y Yin. 2024. "Micromechanical Investigation of the Aging Mechanism in Sand." *Computers and Geotechnics* 175: Paper 106710.

Lukas, R. G. 1986. "Dynamic Compaction for Highway Construction, Volume 1: Design and Construction Guidelines", FHWA Report RD-86/133. Federal Highway Administration.

Lukas, R. G. 1995. "Geotechnical Engineering Circular No. 1: Dynamic Compaction, Publication No. FHWA-SA-95-037", Federal Highway Administration.

Schmertmann, J H. 1991. "The Mechanical Aging of Soils." *Journal of Geotechnical Engineering, ASCE* 117 (9): 1288-1330.

Varaksin, S, B Hamidi, and E D'Hiver. 2005. "Pressuremeter Techniques to Determine Self Bearing Level and Surface Strain for Granular Fills after Dynamic Compaction." In *Int Sym 50 Years of Pressuremeters (ISP5-Pressio 2005), Marne-la-Vallee, France, 22-24 August.*